Antenna Array Design for Mono-Static ISAC

Alexander Felix*[†], Silvio Mandelli*, Marcus Henninger*[†], and Stephan ten Brink[†]
*Nokia Bell Labs Stuttgart, 70469 Stuttgart, Germany
[†]Institute of Telecommunications, University of Stuttgart, 70569 Stuttgart, Germany
E-mail: alexander.felix@nokia.com

Abstract—Mono-static sensing operations in Integrated Sensing and Communications (ISAC) require joint beamforming operations between transmitter and receiver, according to all the considerations already done in the radar literature about coarray theory. In contrast to pure radar systems, ISAC requires to fulfill communications tasks and to retain the corresponding design constraints for at least one half-duplex array. This shifts the available degrees of freedom to the design of the second half-duplex array, that completes the mono-static sensing setup of the ISAC system. Therefore, it is necessary to translate the analysis from the radar literature for the design of sparse arrays to the new ISAC paradigm in order to provision such systems.

Accordingly, we propose a model to evaluate the angular capabilities of an ISAC setup, constrained to the shape of the communications array and its topology requirements. Our analysis is validated by simulation experiments, confirming the value of our model in providing system designers with a tool to drastically improve the trade-off between angular capabilities for sensing and the cost of the deployed hardware. Finally, we discuss possible enhancements to the cellular standards to fully leverage the angular capabilities of such mono-static ISAC systems.

I. Introduction

The first vision papers on sixth generation (6G) wireless network standards were published by the industry a few years ago [1]. From the beginning, future 6G networks promise to further enhance throughput, latency, and reliability performance, while reducing their costs, becoming energy efficient [2], and pushing their reach beyond their initial scope, delivering Integrated Sensing and Communications (ISAC). Even though 6G has not been standardized yet, first works have already started to comment on ISAC feasibility and fundamental limits [3], [4]. Backing the first considerations up with real world results, a first ISAC demonstrator based on communications hardware has been published in [5], with two almost co-located mmWave panels jointly operating to sense the environment.

The task for such a dual array setup is to properly design the joint beamforming capabilities to optimize the angular performance [6]. For a mono-static radar, a desired set of beamforming coefficients can be defined to achieve specific angular metrics such as resolution and sidelobe suppression. To convert a set of desired beamforming coefficients to the physical elements of the arrays, various algorithmic approaches exist,

This work has been submitted to the IEEE for possible publication. Copyright may be transferred without notice, after which this version may no longer be accessible.

such as the later used alternating minimization [7], Riemannian optimization [8], or majorization minimization [9].

To optimize a system's angular capabilities, sparse arrays with element spacing greater than half the wavelength can be used, as demonstrated under the constraint of full duplex operation [10], [11]. However, when integrating sensing functionalities into cellular systems, it is necessary for wireless communications to avoid grating lobes. Therefore, to ensure transmission, the distance between elements of a single full-duplex transmitter should be roughly half the wavelength [12]. To combine both imaging and communications, this leads to the need for alternative approaches to identical arrays [13].

Our work aims to optimize angular capabilities without compromising established wireless communications capabilities. We propose the use of two dedicated arrays for each task in a mono-static setup. The main array primarily adheres to the latest 5G NR hardware specifications, while the second sniffer array addresses the prerequisites for sensing use cases. Thus, the design comprises dissimilar arrays with a uniform communications array having an inter-element spacing of approximately half the wavelength and a sparse sensing array with a larger inter-element spacing. The split of the arrays allows for almost co-located placement, as in a first ISAC demonstrator [5], enabling the shift from full-duplex assumptions to half-duplex operation. Moreover, we validate the feasibility of our approach through a simulation study and investigate the necessary cellular standards enhancements to support the operations of dissimilar arrays. The design approach enables seamless integration with existing communications hardware, while implementing new sensing features with minimal cost impact.

II. SYSTEM MODEL

We consider a narrowband, mono-static wireless network system, like the one depicted in Figure 1. Even though in practice a wireless network is not narrowband, the impact in terms of beam squinting is typically negligible, since the operating carrier bandwidth is narrow compared to the carrier frequency [3]. There are two options to achieve this mono-static setup: operating a single array in full-duplex mode or co-locating two arrays and operating them in half-duplex mode. This paper focuses on the latter, where we assume the angular and beamforming perspective to be co-located, which has been proven to work in practice [5]. One array is designated for communications, while the other specifically

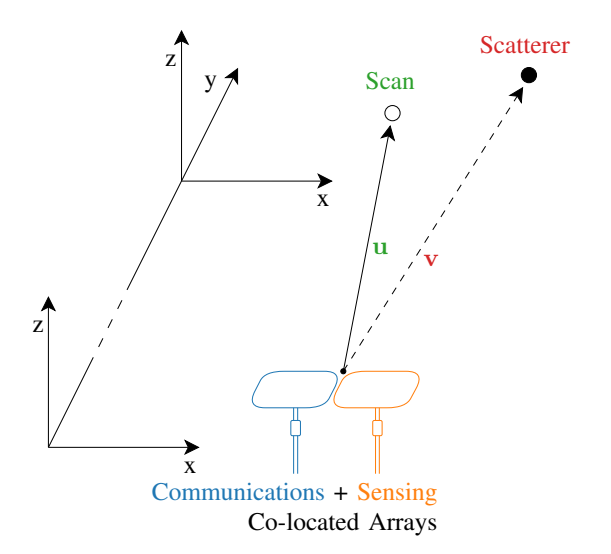


Fig. 1: Schematic of mono-static setup with communications (Tx) and sensing array (Rx) with scan direction \mathbf{u} and scatterer direction \mathbf{v} .

serves as a sniffer for sensing. Both arrays are Uniform Rectangular Arrays (URAs) with shape $\mathcal{S}=N_x\times N_z$ and $N=N_xN_z$ total elements, where N_x and N_z denote the number of elements in horizontal and vertical array direction, respectively. To ease notation, but without loss of generality, we consider arrays with antenna spacing d in both directions. Parameters associated with the communications array as the transmitter and the sensing array as the receiver are denoted with superscripts (c) and (s). However, they can exchange roles without affecting the validity of our approach.

The matrix $\mathbf{P} = [\mathbf{p}_1, \mathbf{p}_2, ..., \mathbf{p}_N]^T \in \mathbb{R}^{N \times 2}$ comprises the normalized element positions, with elements $\mathbf{p}_n = [x_n, z_n]^T$. Under far-field assumption, the relative direction vectors are

$$\mathbf{u} = \left[\cos(\phi)\cos(\theta), \cos(\phi)\sin(\theta)\right]^{\mathrm{T}}, \tag{1}$$

where elevation ϕ and azimuth θ denote the incident angle with regard to the arrays.

A. Normalized Angular Frequency

When evaluating the two-dimensional (2D) angular response of point scatterers in the radian domain, their observed shape depends on the relative angles to their locations. To ensure invariant point scatterer observations regardless of their position in the sampling space, we utilize the Normalized Angular Frequency (NAF) domain [12] instead of the radian domain. Therefore, we express the incident angles ϕ and θ as their NAF equivalents in vertical and horizontal array directions, denoted by η and ℓ , respectively. The equations for the conversions are

$$\eta = \frac{d}{\lambda}\sin\left(\phi\right) , \qquad (2)$$

$$\ell = \frac{d}{\lambda} \frac{\sin(\theta)}{\cos(\phi)} \,. \tag{3}$$

We sample the NAF domain in the interval $[-d/\lambda, d/\lambda]$ to avoid aliases, as suggested in [12]. Note that to cover the full angular domain aperture spanned by the antenna planar array

without aliases, i.e., π , one should use the well-known formula for the maximum antenna distance, i.e., $d < \lambda/2$.

B. Joint Beamforming and Point Spread Function

To perform joint beamforming, it is necessary to define the beamforming coefficient of a single element $w^{(\cdot)}$, whether physical or virtual. These coefficients are then aggregated per array in $\mathbf{W}^{(\cdot)} \in \mathbb{C}^{N_x^{(\cdot)} \times N_z^{(\cdot)}}$. Assuming narrowband conditions for K arbitrary scanned directions, the steering matrix of the array $\mathbf{A}^{(\cdot)} \in \mathbb{C}^{N^{(\cdot)} \times K}$, also denoted as angular response of the scenario, is defined. With $k_0 = 2\pi/\lambda$ as the wavenumber and λ as the wavelength of the center frequency ω_0 , the angular response is expressed as $\mathbf{A}^{(\cdot)} = [e^{-jk_0\mathbf{P}\mathbf{v}_1}, ..., e^{-jk_0\mathbf{P}\mathbf{v}_K}]$.

Based on these definitions, the Point Spread Function (PSF) is given as

$$\psi^{(\cdot)} = \mathbf{A}^{(\cdot)\mathrm{T}} \mathrm{vec} \left(\mathbf{W}^{(\cdot)} \right) , \qquad (4)$$

where $\operatorname{vec}(\cdot)$ denotes the vectorization operator. The PSF expresses the spatial impulse response to a single point scatterer in direction $\mathbf{v} \in \mathbb{R}^2$ of a linear imaging system when the system is steered in scan direction $\mathbf{u} \in \mathbb{R}^2$. This definition allows to determine the system's achievable resolution and sidelobe suppression capabilities. For the joint system of the communications and the sensing array, the effective steering effects of all elements need to be considered. This can be derived from the Khatri-Rao product of the steering matrices of both arrays as

$$\mathbf{A} = \mathbf{A}^{(c)} \odot \mathbf{A}^{(s)} , \qquad (5)$$

which denotes the compound steering matrix of the setup.

C. Antenna Array Model and Sum Co-Array

ISAC arrays should be dimensioned w.r.t. each scenario. In this work, we assume that we are operating with a predetermined communications array based on required communications beamforming capabilities. Thus, we are left with the need to design the sensing array to achieve the desired angular resolution and imaging performance of the sensing tasks.

We define a coherent imaging task in scan direction u according to the following equation

$$\hat{\mathbf{A}}(\mathbf{u}) = \int \mathbf{A}(\mathbf{v}) \ \psi^{(c)}(\mathbf{u}, \mathbf{v}) \ \psi^{(s)}(\mathbf{u}, \mathbf{v}) \ d\mathbf{v}$$

$$= \int \mathbf{A}(\mathbf{v}) \sum_{n=1}^{N^{(c)}} \sum_{i=1}^{N^{(s)}} w_n^{(c)} w_i^{(s)} e^{-jk_0(\mathbf{u} - \mathbf{v})^c \left(\mathbf{p}_n^{(c)} + \mathbf{p}_i^{(s)}\right)} d\mathbf{v} ,$$
(6)

where the multiplication term of $\psi^{(c)}$ and $\psi^{(s)}$ results in the effective joint PSF. Equation (6) defines the sum coarray virtual structure, which contains every possible position $(\mathbf{p}^{(c)} + \mathbf{p}^{(s)})$ and it is denoted with superscript (+) henceforth.

III. IMAGING SETUP FOR ISAC DEPLOYMENTS

In this Section we first introduce prior art's beamforming considerations to jointly operate transmit and receive arrays to achieve a desired PSF. Then, we introduce our proposal for ISAC to work with dissimilar arrays.

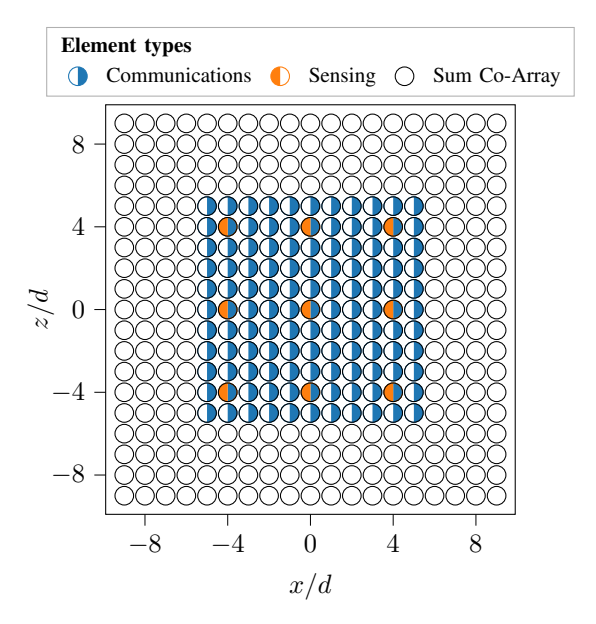


Fig. 2: Sum co-array of dissimilar URAs derived from a communications array of $\mathcal{S}^{(c)} = 11 \times 11$ with $d^{(c)} = \lambda/2$, and a sparse sensing array of $\mathcal{S}^{(s)} = 3 \times 3$ with $d^{(s)} = 2\lambda$.

A. Beamforming Considerations from Prior Art

As demonstrated in [13], a desired PSF derived from arbitrary beamforming coefficients can be obtained by two identical arrays with sparse element distribution. The achievable PSF is determined by the shape of the sum co-array, meaning that different physical arrays can achieve the same angular capabilities. As an example, consider a Uniform Linear Array (ULA) with N=11 elements and $d=\lambda/2$, compared to a Minimum Redundancy Array (MRA) of N=7 and irregular spacing. The MRA is the array structure with the minimum number of elements that achieves the same sum co-array as a uniform array [14]. Therefore, for both cases, we obtain a ULA sum co-array with 21 elements and $d=\lambda/2$.

To determine the beamforming coefficients, we adopt the approach of prior works [13], [15]. We first derive the PSF by an arbitrary beamforming coefficient set for the given sum coarray and then try to obtain the same effect by mapping these weights to multiple joint transmitter and receiver acquisitions Q. The beamforming weights are determined by an alternating minimization algorithm and the final image is obtained by an ad-hoc weighted "image addition" technique. The minimum Q required for algorithmic convergence is correlated with the total number of elements N and the sparseness of the arrays.

B. Dissimilar Arrays for ISAC Operations

It has been proven that similar PSFs (and hence angular performance) can be achieved with fewer elements, e.g. comparing MRAs to ULAs of greater element number. However, to avoid grating lobes, communications hardware must operate in either transmit or reception mode with constant spacing close to $\lambda/2$ [12]. As a result, the complementary sensing part can be optimized as full duplex of the operating elements or as a separate, almost co-located array while keeping the

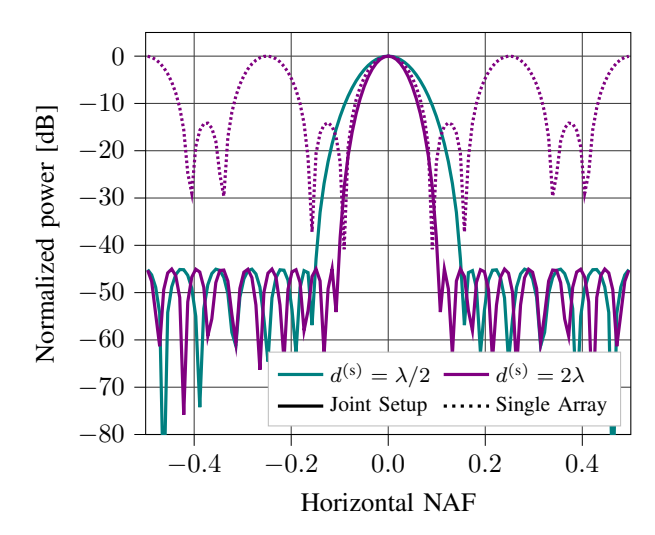


Fig. 3: PSF comparison: Single sparse array $\mathcal{S}^{(s)} = 3 \times 3$ with $d^{(s)} = 2\lambda$ vs. joint setup of fixed communications array $\mathcal{S}^{(c)} = 11 \times 11$ with $d^{(c)} = \lambda/2$ spacing and varying sensing array.

communications array fixed. The latter differs from previous work on MRAs that assumed a perfect full duplex setup [11].

Thus, one array follows the existing and future requirements of 6G communications. The second array, or sensing array, aims to limit the number of elements while maintaining the imaging performance of a larger array. Such a joint setup is shown in Figure 2, with a communications array of $\mathcal{S}^{(c)} = 11 \times 11$ elements and $d^{(c)} = \lambda/2$ spacing and a sensing array of $\mathcal{S}^{(s)} = 3 \times 3$ elements and $d^{(s)} = 2\lambda$. In this example, we obtain a sum co-array of $\mathcal{S}^{(+)} = 19 \times 19$ compared to $\mathcal{S}^{(+)} = 12 \times 12$ of the reference case with $d^{(s)} = \lambda/2$.

Considering only the sparse $\mathcal{S}^{(s)}=3\times 3$ sensing array, we can obtain the PSF shown in Figure 3 as the dotted line curve in purple color. Here, we can see the grating lobes generated due to $d^{(s)}\gg \lambda/2$, which are detrimental to our imaging task. Therefore, we consider the joint beamforming operations of the two arrays, plotting their PSFs with solid lines. Moreover, the main lobe can be significantly narrowed as $d^{(s)}$ – and thus also the aperture of the sum co-array – is increased.

The example in the previous section highlights the potential of leveraging arrays with $d^{(s)}\gg \lambda/2$ in joint beamforming operations with conventional uniform arrays with $d^{(c)}=\lambda/2$. In Figure 4, we further extend our investigation to the 2D NAF domain by comparing the response of a scenario with two point scatterers, with three different $d^{(s)}$ values. We note a decreasing main lobe width when the antenna spacing $d^{(s)}$ increases. However, noise enhancement effects become noticeable when the spacing exceeds a certain threshold, specifically for (c) with $d^{(s)}=4\lambda$. We observed that this is caused by bad convergence of the alternating minimization algorithm. Therefore, it is important to find a trade-off between spacing and noise enhancement.

C. Impacts in Cellular Standards

In the previous part of this section we discussed dimensioning of the sensing array for a mono-static ISAC system. In this subsection we consider some requirements in cellular

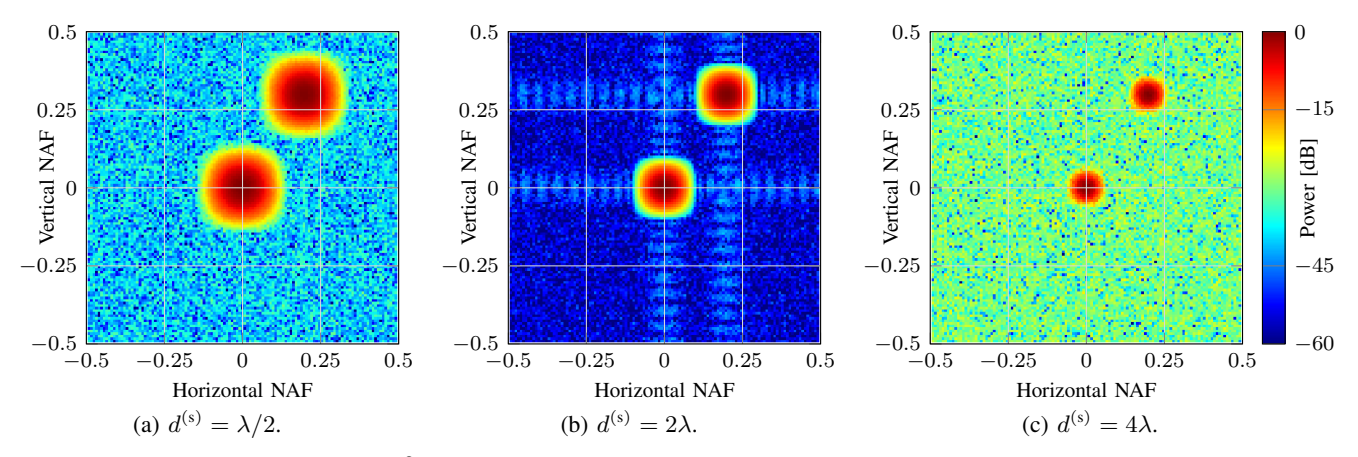


Fig. 4: Intensity plot over 2D NAF for $\sigma^2 = -10$ dB observing 2 point scatterers for different joint arrays. The communications array is fixed with $\mathcal{S}^{(c)} = 11 \times 11$ and $d^{(c)} = \lambda/2$, while the sensing array has fixed $\mathcal{S}^{(s)} = 3 \times 3$ but varying $d^{(c)}$.

standards to support related sensing operations, making use of the angular capabilities of each operating mono-static system.

With ISAC being on the roadmap for 6G, current cellular standards support active user positioning. The NR Positioning Protocol A (NRPPa) [16] controls the message exchange between the location management function (LMF) in the core network and each Transmission Reception Point (TRP) of the base stations. NRPPa already allows for a TRP to signal its angular beamforming capabilities to the LMF, accounting for its half-duplex single array topology and the configured beamforming of each signal transmission for positioning purposes.

However, it is not envisioned to signal the joint transmit/receive beamforming capabilities of a mono-static ISAC system in combination to any existing management function (MF), e.g., the LMF. Thus, we suggest to develop a framework to support signalling of the beamforming capabilities of a mono-static system with multiple co-located arrays to the MF, which can be realized with a new MF or an extension to the LMF to support sensing. We propose to add to the TRP capabilities report also the information that the TRP can operate as a mono-static sensing system and its corresponding angular capabilities. As we have shown, the joint transmit/receive angular capabilities are better than what a single half-duplex array can offer. Alternatively, two co-located TRPs can signal the LMF that they can operate together as a mono-static ISAC system, sharing similar information. We believe that such standard enhancements are necessary to allow the MF to properly provision sensing measurements in ISAC deployments.

IV. SIMULATION STUDIES

To compare different sensing array design options, we perform a Monte Carlo simulation study in which we place two point scatterers in the 2D NAF space. The first scatterer is placed randomly, while the second is placed on the 2D NAF plane with a fixed Euclidean distance $\Delta d^{(P)}$, but at a random direction relative to the first. By varying $\Delta d^{(P)}$, we analyze the ability of the system to discriminate between multiple targets, i.e., its resolution. The joint setups investigated consist of two URAs with a communications array used as

transmitter with fixed $\mathcal{S}^{(c)}=11\times 11$ and $d^{(c)}=\lambda/2$ element spacing. The sensing panel used as receiver varies in the number of antenna elements, leading to three array shapes $\mathcal{S}^{(s)}=\{3\times 3,5\times 5,7\times 7\}$, which are permuted with three different element spacings $d^{(s)}=\{\lambda/2,\,3\lambda/2,\,2\lambda\}$.

To reconstruct the image of a scenario, we use the transposed representation of Eq. (6) in matrix operations. A single acquisition of the joint transmitter and receiver beamforming task is denoted by index q. For the q-th acquisition, acquired in the desired direction \mathbf{u} , this yields

$$y_q(\mathbf{u}) = \mathbf{w}_q^{(s)T}(\mathbf{u}) \mathbf{A}^{(s)} \mathbf{\Gamma} \mathbf{A}^{(c)T} \mathbf{w}_q^{(c)}(\mathbf{u}) + \mathbf{w}_q^{(s)T}(\mathbf{u}) \mathbf{n}_q$$
, (7)

where the complex circular Additive White Gaussian Noise (AWGN) \mathbf{n}_q has zero mean and covariance matrix $\sigma^2\mathbf{I}_2$, with \mathbf{I}_2 being a 2×2 identity matrix. Further, the coefficients of the K scatterers with constant amplitude and uniform random phase in the interval $[0,2\pi)$ are represented by a diagonal matrix $\mathbf{\Gamma}\in\mathbb{C}^{K\times K}$. A pixel of the complete image acquired in the direction \mathbf{u} is obtained by the summation of all Q joint beamforming acquisitions

$$y(\mathbf{u}) = \sum_{q=1}^{Q} y_q(\mathbf{u}) . \tag{8}$$

Once the reconstructed image of the scenario has been acquired, targets are detected using Constant False Alarm Rate (CFAR) thresholding with a desired probability of false alarm $P^{(\text{FA})}=10^{-3}$ [17]. Peaks above the CFAR threshold are detected and sorted by strength. One by one, their estimation is improved using interpolation techniques. With this position, their effect is removed from the image using the techniques described in the multiple targets section of [12].

In our simulations with different permutations of the sensing array, we measure performance in terms of target missed detection probability $P^{(\text{MD})}$ and Root Mean Squared Error (RMSE) of angular estimation. More details about the simulation parameters are given in Table I. For a peak to be considered a detection, it must fall within a range ρ around a true target. The range is determined by the resolution of the arrays, which depends on their physical size and the

TABLE I. SIMULATION PARAMETERS AND ASSUMPTIONS

| Parameter | Value / Description |
|--|---|
| communications array shape $\mathcal{S}^{(c)}$ | 11 × 11 |
| communications array spacing d(c) | $\lambda/2$ |
| Number of targets | 2 |
| Target reflection coefficients | $e^{j\Phi_s}$, where $\Phi_s \backsim U[0,2\pi)$ |
| Distribution of beamforming coefficients | Chebyshev window |
| Chebyshev attenuation $\Omega^{(C)}$ | 45 dB |
| Detection method | Interpolated CFAR |
| | Target cancellation as in [12] |
| Desired $P^{(FA)}$ of CFAR | 10^{-3} |
| Iterations per data point L | 1000 |

beamforming coefficients used. A Chebyshev window with $\Omega^{(C)}=45$ dB sidelobe attenuation is used as the desired set of beamforming coefficients, resulting in a sidelobe factor of $r=1/\left(10^{\Omega^{(C)}/20}\right)$ [18]. Then, we calculate the half mainlobe width of the angular frequency response of the arrays, which, in vertical array direction, is given by

$$\omega^{(z)} = \arccos\left(\frac{1}{\cosh\left(\frac{\arccos(1/r)}{N_z - 1}\right)}\right).$$
 (9)

The resolution can be obtained by scaling the half main-lobe width with the NAF limit of the respective direction, i.e. the resolution in vertical direction is given by

$$\rho^{(z)} = \frac{d}{\lambda}\omega^{(z)} \ . \tag{10}$$

In our case, the NAF limit corresponds to the sum co-array spacing $d/\lambda=0.5$. For the horizontal element direction, $\rho^{(x)}$ can be derived analogously from $\omega^{(x)}$ as a function of N_x .

To compute the RMSE, only the closest detected target with distance $\Delta d^{(E)}$ to the true target is evaluated. This, combined with the number of iterations L, gives the following equation

NAF RMSE =
$$\sqrt{\frac{\sum_{i=1}^{L} (\Delta d^{(E)})^2}{L}}$$
 . (11)

Furthermore, if no peak is detected within the resolution range ρ around a true target, we assign a penalty of 2ρ instead.

In Figure 5 we plot results with different noise power $\sigma^2 = \{-10, 0, 10\}$ dB, deploying the sensing URA with different numbers of elements and antenna spacing, represented by different colors and line styles, respectively.

Comparing the probability of missed detection $P^{(\mathrm{MD})}$ curves in Figures 5a, 5b and 5c, it is evident that the curves break down at a specific distance between the scatterers $\Delta d^{(\mathrm{P})}$, indicating the resolution limits of the respective array setup. One can further notice that increasing the number of elements improves performance by reducing the resolution limit to a lower $\Delta d^{(\mathrm{P})}$. Comparing performance also with different antenna spacing, it is apparent that setups with smaller $d^{(\mathrm{S})}$ outperform arrays with more elements but smaller spacing. For example, the dotted violet curve of $\mathcal{S}=3\times3$ and $d^{(\mathrm{S})}=2\lambda$ outperforms the solid green curve of $\mathcal{S}=5\times5$ and $d^{(\mathrm{S})}=\lambda/2$ over the full noise power range. This finding allows the

deployment of sensing arrays with fewer elements, requiring less computational complexity and ultimately resulting in cheaper solutions while still achieving the same resolution. Conversely, for similar costs, the resolution performance can be significantly improved. This can be observed by comparing curves with the same colours but different line styles.

The lower row of Figure 5 shows the RMSE of the targets' NAF estimation. From the increased RMSE values it is apparent that the target interference is greater for smaller $\Delta d^{(P)}$. The curves drop to a floor due the noise introduced by the constant AWGN channel and the additional noise enhancement effects of the image addition once the resolution limits of our setups are reached. When considering the color of the curves, it is noticeable that increasing the number of elements in the sensing arrays causes the RMSE to break down earlier. As noted earlier with $P^{(MD)}$, the RMSE evaluation also indicates that arrays with fewer elements but larger spacing outperform arrays with more elements but smaller spacing. Apart from these observations, the RMSE increase for smaller spacings may seem counter-intuitive. However, this effect is likely due to evaluating only the smallest distance between a single detected peak and the true target in a scenario with two targets.

Examining the relationship between $P^{(\text{MD})}$ and the number of elements for the same spacing in Figure 5c, it appears that the light blue curve with $\mathcal{S}^{(\text{s})} = 11 \times 11$ and $d^{(\text{s})} = \lambda/2$ is anomalous. This is likely due to a convergence issue with the alternating minimization algorithm used based on [13].

V. CONCLUSION

In this work, we propose and analyze dissimilar array setups to realize first half-duplex ISAC base stations, integrating an ad-hoc sensing array with the legacy communications one, with the latter constrained to have an element spacing close to half the carrier wavelength. Hence, we can improve the angular capabilities of the compound setup only by increasing the antenna spacing of the sniffer array. As a result, the joint setup operates with fewer antenna elements and obtains a better performance versus cost trade-off. Moreover, this can ease the shift from full-duplex demands to half-duplex functionality of almost co-located arrays, which can be achieved using radio equipment closer to those currently deployed.

After describing the enhancements needed in the 6G standard to better support mono-static base station deployments, we complement our study with numerical evaluations of our dissimilar arrays setup. The results confirm the expected gains, demonstrating increased resolution performance of systems that are optimized for such setups, i.e., with higher antenna spacing, compared to legacy communications-only arrays.

Next steps include further analysis of convergence issues and noise enhancement effects identified during our studies, resulting from the algorithms used to determine the beamforming coefficients. We plan to address these matters alongside an extension of our analysis to a broadband signal model.

ACKNOWLEDGMENT

The authors would like to thank Thorsten Wild, Harish Viswanathan, and Paolo Tosi for their insightful comments.

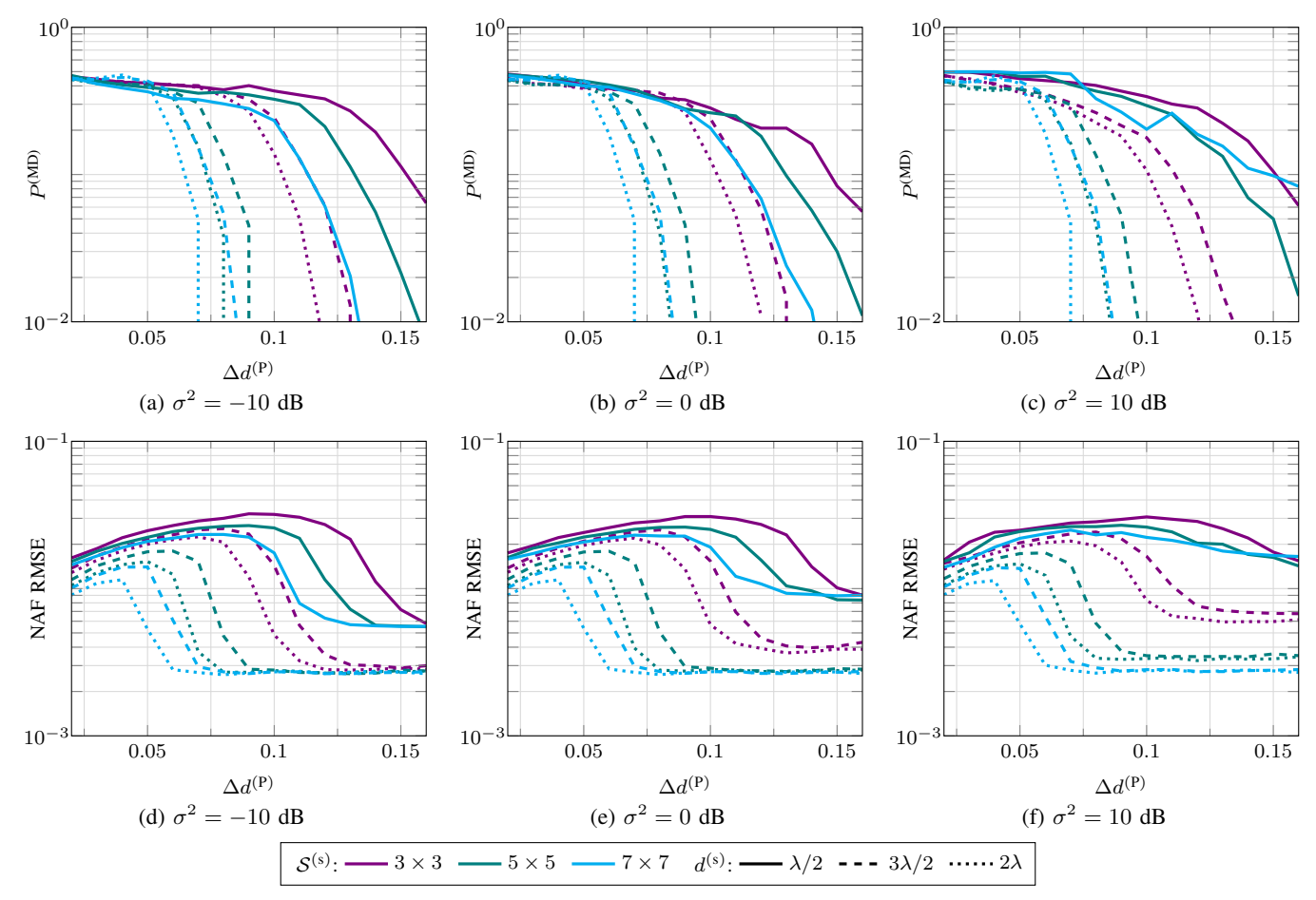


Fig. 5: Resolution capabilities of joint, dissimilar arrays for varying noise powers are evaluated for probability of missed detection and RMSE. The communications array has fixed shape $S^{(c)} = 11 \times 11$ with $d^{(c)} = \lambda/2$ and the sensing array is varied according to legend.

This work was developed within the KOMSENS-6G project, partly funded by the German Ministry of Education and Research under grant 16KISK112K.

REFERENCES

- [1] H. Viswanathan and P. E. Mogensen, "Communications in the 6G era," *IEEE Access*, vol. 8, pp. 57063–57074, Aug. 2020.
- [2] S. Wesemann, J. Du, and H. Viswanathan, "Energy efficient extreme MIMO: design goals and directions," *IEEE Communications Maga*zine, vol. 61, no. 10, pp. 132–138, Nov. 2023.
- [3] S. Mandelli, M. Henninger, M. Bauhofer, and T. Wild, "Survey on integrated sensing and communication performance modeling and use cases feasibility," in 2023 2nd International Conference on 6G Networking (6GNet), Oct. 2023, pp. 1–8.
- [4] A. Liu et al., "A survey on fundamental limits of integrated sensing and communication," *IEEE Communications Surveys & Tutorials*, vol. 24, no. 2, pp. 994–1034, Feb. 2022.
- [5] T. Wild, A. Grudnitsky, S. Mandelli, M. Henninger, J. Guan, and F. Schaich, "6G Integrated Sensing and Communication: From Vision to Realization," in 2023 20th European Radar Conference (EuRAD), Sep. 2023, pp. 355–358.
- [6] R. T. Hoctor and S. A. Kassam, "The unifying role of the coarray in aperture synthesis for coherent and incoherent imaging," *Proceedings of the IEEE*, vol. 78, no. 4, pp. 735–752, Apr. 1990.
- [7] X. Yu, J.-C. Shen, J. Zhang, and K. B. Letaief, "Alternating Minimization Algorithms for Hybrid Precoding in Millimeter Wave MIMO Systems," *IEEE Journal of Selected Topics in Signal Processing*, vol. 10, no. 3, pp. 485–500, Apr. 2016.
 [8] B. Wang, Z. Cheng, and Z. He, "Manifold optimization for hybrid
- [8] B. Wang, Z. Cheng, and Z. He, "Manifold optimization for hybrid beamforming in dual-function radar-communication system," *Multidimensional Syst. Signal Process.*, vol. 34, no. 1, p. 1–24, Sep. 2022.

- [9] A. Arora, C. G. Tsinos, B. S. M. R. Rao, S. Chatzinotas, and B. Ottersten, "Hybrid Transceivers Design for Large-Scale Antenna Arrays Using Majorization-Minimization Algorithms," *IEEE Transactions on Signal Processing*, vol. 68, pp. 701–714, 2020.
- [10] A. Koc, "Hybrid Beamforming Techniques in Full-Duplex/Half-Duplex Massive MIMO Wireless Communications," Ph.D. dissertation, McGill University, 2022.
- [11] D. Hu, X. Wei, M. Xie, and Y. Tang, "A Sparse Shared Aperture Design for Simultaneous Transmit and Receive Arrays with Beam Constraints," *Sensors*, vol. 23, no. 12, p. 5391, Jan. 2023.
- [12] S. Mandelli, M. Henninger, and J. Du, "Sampling and reconstructing angular domains with uniform arrays," *IEEE Transactions on Wireless Communications*, Nov. 2022.
- [13] R. Rajamäki, S. P. Chepuri, and V. Koivunen, "Hybrid beamforming for active sensing using sparse arrays," *IEEE Transactions on Signal Processing*, vol. 68, pp. 6402–6417, Oct. 2020.
- [14] F. Schwartau, Y. Schröder, L. Wolf, and J. Schoebel, "Large Minimum Redundancy Linear Arrays: Systematic Search of Perfect and Optimal Rulers Exploiting Parallel Processing," *IEEE Open Journal of Antennas and Propagation*, vol. 2, pp. 79–85, Dec. 2020.
- [15] R. Rajamäki, S. P. Chepuri, and V. Koivunen, "Analog beamforming for active imaging using sparse arrays," in 2019 53rd Asilomar Conference on Signals, Systems, and Computers, 2019, pp. 1202–1206.
- [16] 3GPP, "NG-RAN; NR Positioning Protocol A (NRPPa)," Technical Specification (TS) 38.455, 2024, version 18.0.0.
- [17] M. A. Richards, J. A. Scheer, and W. A. Holm, *Principles of Modern Radar: Basic Principles*. Raleigh, NC, USA: SciTech Pub., 2010.
- [18] P. Lynch, "The Dolph-Chebyshev Window: A Simple Optimal Filter," Monthly Weather Review, vol. 125, no. 4, pp. 655-660, Apr. 1997.